

Research Article

Open Access



Dependence of microwave dielectric properties on ceramic connectivity in ultralow- ϵ_r Al_2O_3 porous ceramics

Xiao Jian Yan, Meng Cao, Lei Li , Shu Ya Wu, Xiang Ming Chen

Laboratory of Dielectric Materials, School of Materials Science and Engineering, Zhejiang University, Hangzhou 310058, Zhejiang, China.

Correspondence to: Dr. Lei Li, Laboratory of Dielectric Materials, School of Materials Science and Engineering, Zhejiang University, 866 Yuhangtang Road, Hangzhou 310058, Zhejiang, China. E-mails: zjulilei@zju.edu.cn; Dr. Shu Ya Wu, Laboratory of Dielectric Materials, School of Materials Science and Engineering, Zhejiang University, 866 Yuhangtang Road, Hangzhou 310058, Zhejiang, China. E-mail: wushuya@zju.edu.cn

How to cite this article: Yan, X. J.; Cao, M.; Li, L.; Wu, S. Y.; Chen, X. M. Dependence of microwave dielectric properties on ceramic connectivity in ultralow- ϵ_r Al_2O_3 porous ceramics. *Microstructures* 2025, 5, 2025065. <https://dx.doi.org/10.20517/microstructures.2024.202>

Received: 31 Dec 2024 **First Decision:** 20 Feb 2025 **Revised:** 18 Mar 2025 **Accepted:** 28 Mar 2025 **Published:** 9 May 2025

Academic Editor: Dae-Yong Jeong **Copy Editor:** Fangling Lan **Production Editor:** Fangling Lan

Abstract

Introducing pores is an effective approach for fabricating ultralow- ϵ_r ceramics; however, it is still unclear how the microstructures affect the microwave dielectric properties. In the present work, Al_2O_3 -A and Al_2O_3 -B porous ceramics were prepared by incomplete sintering at 1,000-1,650 °C and sintering at 1,650 °C with a porogen, respectively, so that the effects of porosity and ceramic connectivity can be clarified. The introduction of pores led to a significant decrease in ϵ_r , Qf , and $|\tau_f|$, and Al_2O_3 -B ceramic exhibits a slightly higher ϵ_r , a larger $|\tau_f|$, and a much higher Qf value compared to the Al_2O_3 -A counterpart with a similar relative density. For Al_2O_3 -A, increasing the sintering temperature and relative density notably enhanced ceramic connectivity, while Al_2O_3 -B's ceramic connectivity remained relatively insensitive to density variations. The improved ceramic connectivity in Al_2O_3 -B enhanced the contribution of the ceramic phase to ϵ_r and τ_f , while also increased the Qf value by reducing ceramic-pore interfaces. Notably, Al_2O_3 -B, with a low relative density of 48.31%, demonstrated a good combination of microwave dielectric properties, with $\epsilon_r = 4.16$, $Qf = 38,400$ GHz, and $\tau_f = -44.3$ ppm/°C. These findings reveal the strong dependence of microwave dielectric properties on ceramic connectivity in porous ceramics, and also inspire the development of ultralow- ϵ_r materials by regulating both the porosity and ceramic connectivity.

Keywords: Porous ceramics, Al_2O_3 , ceramic connectivity, ultralow dielectric constant, microwave



© The Author(s) 2025. **Open Access** This article is licensed under a Creative Commons Attribution 4.0 International License (<https://creativecommons.org/licenses/by/4.0/>), which permits unrestricted use, sharing, adaptation, distribution and reproduction in any medium or format, for any purpose, even commercially, as long as you give appropriate credit to the original author(s) and the source, provide a link to the Creative Commons license, and indicate if changes were made.



INTRODUCTION

In recent years, the low-dielectric-constant ($\epsilon_r < 10$) and ultralow- ϵ_r ($\epsilon_r < 5$) microwave dielectric ceramics have attracted more and more attention mainly due to the rapid development of microwave communication technology toward higher working frequencies, especially millimeter-wave frequency band^[1–4]. On one hand, for the electromagnetic wave propagating in a dielectric substrate with the length of L , the phase delay is $2\pi fL/(\sqrt{\epsilon_r}c_0)$, where f and c_0 are the frequency and propagating speed of the electromagnetic wave in vacuum, respectively. Therefore, the phase delay increases proportionally with frequency, and it can be suppressed at higher working frequencies only by adopting the substrate materials with lower ϵ_r . On the other hand, microwave dielectric ceramics are also widely used in many key resonating units such as resonators and filters, whose sizes are mainly determined by the ϵ_r ^[3,5]. For microwave communication mainly working at the sub-6 GHz band in the past decades, high- ϵ_r and middle- ϵ_r microwave dielectric ceramics are usually used in these resonating units for minimization^[5]. However, the minimization of devices and components is a natural consequence in millimeter-wave communication due to the rapid decrease in wavelength with frequency, and it is no longer an important aim for the resonating units in most cases. Instead, too small sizes of these resonating units may result in many serious problems, such as difficulty in precise size control and low carrying power. Therefore, low- ϵ_r and ultralow- ϵ_r microwave dielectric ceramics are also urgently demanded in these millimeter-wave resonating units to maintain reasonable and machinable sizes and high carrying power.

In the past decades, many low- ϵ_r microwave dielectric ceramics have been developed, including borates^[6–8], silicates^[9–12], aluminates^[13–15], phosphates^[16–18], molybdates^[19,20], fluorides^[21], and *etc.* However, the ϵ_r is higher than 5 for most of them, and very limited dense inorganic materials exhibit the ϵ_r lower than 5, such as SiO₂ polymorphs^[22,23], borosilicate glass^[24], and cordierite^[25,26]. Till now, amorphous SiO₂ with the ϵ_r of around 3.8 is still the most important and irreplaceable ultralow- ϵ_r inorganic material^[23]. The embarrassing situation for the research and application of ultralow- ϵ_r inorganic materials is attributed to the higher ionic polarization and higher density in comparison with organic materials, both of which tend to increase the ϵ_r ^[4]. Therefore, developing dense inorganic materials with ultralow ϵ_r is a big challenge. An effective approach to reducing the ϵ_r of ceramics is to introduce pores, forming porous ceramics^[27–32], which can be regarded as “ceramic-air” composites. Since air has a very low ϵ_r of around 1 and is nearly lossless, porous ceramics offer a means to widely regulate the three key parameters of microwave dielectric properties: ϵ_r , Qf value, and temperature coefficient of resonant frequency (τ_f)^[2,3]. Moreover, introducing air into microwave dielectric ceramics can lighten microwave devices, lower costs, and improve portability^[33,34].

Although extensive research has been conducted on porous microwave dielectric ceramics, most studies have primarily focused on controlling porosity and its effects on microwave dielectric properties^[27,31,35], while other microstructural factors have often been overlooked. Among these factors, phase connectivity is an important microstructural factor, as it significantly influences the properties of composites and porous materials, such as mechanical properties^[36], electrical and thermal conductivities^[37], and piezoelectric properties^[38]. Our recent work revealed that the ceramic connectivity is also very important for the dielectric properties of BaTiO₃-epoxy composites^[39] and CaTiO₃ porous ceramics^[32] with high ϵ_r , since it dominates the electric field distributed in the constituting phases with the ϵ_r differing much from each other. For the low- ϵ_r and ultralow- ϵ_r porous ceramics, the difference between the ϵ_r of constituting phases (ceramic and air) becomes much less, so the effects of ceramic connectivity may be quite different. Furthermore, previous studies on porous ceramics have mainly addressed dielectric constant and dielectric loss, while little attention has been given to τ_f , a key parameter that determines the temperature stability of microwave dielectric ceramics. Therefore, it is not only of scientific significance but also important for practical application to systematically investigate how porosity and ceramic connectivity affect the ϵ_r , Qf value, and τ_f .

of low- ϵ_r and ultralow- ϵ_r porous ceramics.

Al_2O_3 ceramic is an important low- ϵ_r microwave dielectric ceramic, which exhibits a low ϵ_r around 10, a high Qf value of 330,000–450,000 GHz, and a relatively large negative τ_f of about $-60 \text{ ppm}/^\circ\text{C}$ ^[27,40–42]. Al_2O_3 microwave dielectric ceramic is often adopted as the model material to reveal the effects of a series of factors such as porosity, grain size, impurity, and humidity^[27,40,43]. Therefore, in the present work, two groups of Al_2O_3 porous ceramics with varying porosity and ceramic connectivity were prepared and used as the model materials. The microstructural evolution, microwave dielectric properties, and their dependence on ceramic connectivity were investigated and analyzed.

MATERIALS AND METHODS

Fine $\alpha\text{-Al}_2\text{O}_3$ powder with an average particle size of 200 nm (> 99.9%, Sinopharm Chemical Reagent Co., Ltd.) was used for preparing Al_2O_3 porous ceramics. The raw powder was dried and mixed with 5 wt% polyvinyl alcohol solution as the binder. The powder was uniaxially pressed into compacts with 12 mm in diameter under 100 MPa for 1 min. The compacts were then sintered at different temperatures of 1,000–1,650 $^\circ\text{C}$ for 3 h in air with a heating rate of 5 $^\circ\text{C}/\text{min}$ and a cooling rate of 2 $^\circ\text{C}/\text{min}$, and the as-prepared ceramics were denoted by $\text{Al}_2\text{O}_3\text{-A}$. For $\text{Al}_2\text{O}_3\text{-B}$ porous ceramics, Al_2O_3 powder was mixed with 20–60 vol% NH_4HCO_3 powder (AR, Sinopharm Chemical Reagent Co., Ltd.) as the porogen because NH_4HCO_3 can be decomposed completely at low temperatures without any residual or reaction with Al_2O_3 , and thus does not affect the sintering characteristics. The mixed powder was also pressed into compacts, which were sintered at the optimum temperature of 1,650 $^\circ\text{C}$ for 3 h after heating at 70 $^\circ\text{C}$ for 3 h to decompose NH_4HCO_3 and form large pores.

The bulk density and total porosity of the samples were measured using the geometric method. The open porosity was measured by the Archimedes drainage method, and the closed porosity was calculated from the total porosity and open porosity. The phase constitution of the Al_2O_3 raw powder and porous ceramics was identified by X-ray diffraction (XRD) using Cu K α Radiation (Rigaku 2550/PC, Rigaku, Tokyo, Japan). The microstructure on the fractured surfaces of $\text{Al}_2\text{O}_3\text{-A}$ and $\text{Al}_2\text{O}_3\text{-B}$ ceramics was observed by field emission scanning electron microscopy (SEM, GeminiSEM 300, Carl Zeiss Microscopy GmbH, Germany). The Vickers hardness was measured by a Vickers indentation tester (MHVD-5IS, Shanghai Jujing Precision Instrument Manufacturing), and the measurement for $\text{Al}_2\text{O}_3\text{-B}$ porous ceramics was conducted in the regions far from the large pores. The cylindrical samples with 9.5–12 mm in diameter and 3.8–6 mm in thickness were used to measure the microwave dielectric properties using a vector network analyzer (Agilent E8363B, Agilent Technologies Inc., Santa Clara, CA). The ϵ_r and Qf were measured at 10.2–15.5 GHz by a resonant cavity method^[44]. The τ_f was calculated and corrected from the resonant frequencies measured at 20 and 80 $^\circ\text{C}$ ^[44].

RESULTS AND DISCUSSION

Figure 1 shows the relative density and porosities of $\text{Al}_2\text{O}_3\text{-A}$ ceramics as functions of sintering temperature (T_s). With increasing T_s from 1,000 to 1,300 $^\circ\text{C}$, the relative density of $\text{Al}_2\text{O}_3\text{-A}$ ceramics increases slowly from 41.25% to 46.15%, and the trend speeds up for higher sintering temperatures. The closed porosity is within 5% for all the $\text{Al}_2\text{O}_3\text{-A}$ ceramics, so the total porosity is dominated by the open one. The highest relative density of 91.73% is obtained for the sintering temperature of 1,650 $^\circ\text{C}$. Therefore, the $\text{Al}_2\text{O}_3\text{-B}$ ceramics are sintered at the optimum temperature of 1,650 $^\circ\text{C}$, and Figure 1B shows the relative density and porosities of $\text{Al}_2\text{O}_3\text{-B}$ ceramics as functions of NH_4HCO_3 volume fraction in the green compacts ($V_{\text{NH}_4\text{HCO}_3}$). The relative density of $\text{Al}_2\text{O}_3\text{-B}$ ceramics decreases with $V_{\text{NH}_4\text{HCO}_3}$, and it can be tuned significantly from 78.76% to 48.31% by increasing $V_{\text{NH}_4\text{HCO}_3}$ from 20% to 60%. The decomposition of NH_4HCO_3 particles

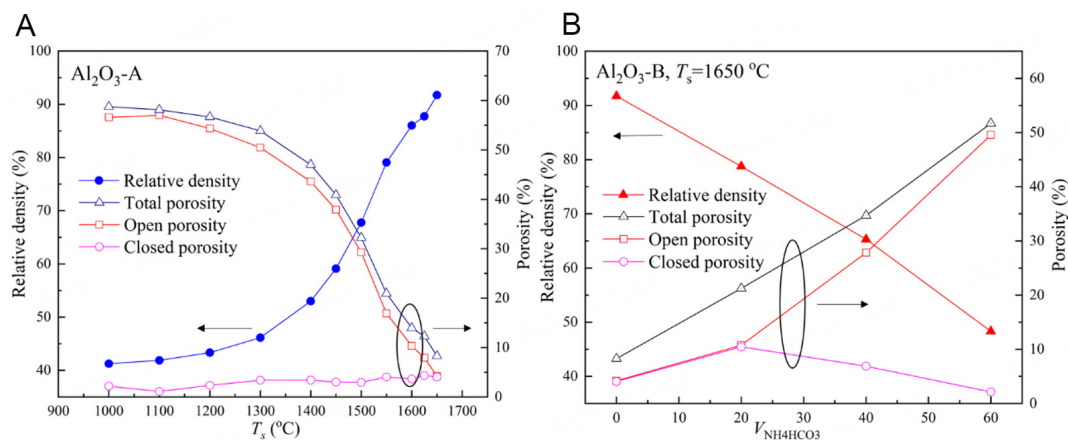


Figure 1. Relative density and porosities of (A) Al₂O₃-A and (B) Al₂O₃-B porous ceramics.

produces large pores, which tend to be separated from one another and, therefore, increase the closed porosity for the low $V_{NH_4HCO_3}$. When $V_{NH_4HCO_3}$ is high, however, the NH₄HCO₃ particles may contact the neighbors, and the decomposition of contacting particles results in the interconnected network of the formed large pores. Therefore, the closed porosity first increases and then decreases with $V_{NH_4HCO_3}$, although the total porosity always increases for Al₂O₃-B ceramics, as shown in Figure 1B. The XRD patterns of Al₂O₃ raw powder and some typical Al₂O₃-A and Al₂O₃-B ceramics are shown in Supplementary Figure 1. These XRD patterns are almost the same, and all the peaks can be indexed by α -Al₂O₃ (PDF card: 97-003-3639), indicating that the sintering temperature and porosity have no effect on the phase constitution and crystal structure.

The SEM images of the fractured surfaces of Al₂O₃-A [Figure 2] and Al₂O₃-B [Figure 3] ceramics clearly reveal the significant difference between the microstructures of the two groups of Al₂O₃ ceramics. When the sintering temperature is as low as 1,000 °C, the small and rounded particles with a size of around 200 nm and their aggregations are observed in Al₂O₃-A, which inherits the microstructure of Al₂O₃ raw powder. The microstructure does not change much at a sintering temperature of 1,200 °C, except that the aggregations become more clear, which is consistent with the slowly increasing relative density shown in Figure 1A and indicates the initial stage of sintering. A significant microstructural evolution can be observed at a sintering temperature of 1,400 °C, at which the original particles with round shapes disappear. Instead, the particles become a little larger and their edges are somewhat sharp, indicating the appearance of initial grains. Furthermore, the initial grains are bonded to some extent and the sintering necks between grains appear, although a lot of small pores seem to hinder the bonding of grains. With further increase in the sintering temperature up to 1,600 °C, the grains with sharp edges and the bonding between neighbored grains become more distinct, together with significant grain growth, clear grain boundaries, and exclusion of pores. Here, connectivity is employed to represent the phase continuity or degree of interconnection within a phase. For the present Al₂O₃ porous ceramics, the ceramic connectivity refers to the extent of bonding between Al₂O₃ particles or grains. Therefore, the above discussion reveals that the connectivity of ceramic phase is enhanced with relative density when the sintering temperature increases from 1,000 to 1,600 °C. The microstructure changes little at a higher sintering temperature of 1,650 °C, except that the pores continue to decrease, indicating the final stage of sintering. Additionally, the average grain size increases with sintering temperature from 0.44 to 4.23 μ m, as shown in Figure 4, and the grain size distribution is illustrated in Supplementary Figure 2. In comparison, the microstructure changes very differently with relative density for Al₂O₃-B ceramics, as shown in Figure 3. The large pores with the size of several to tens of

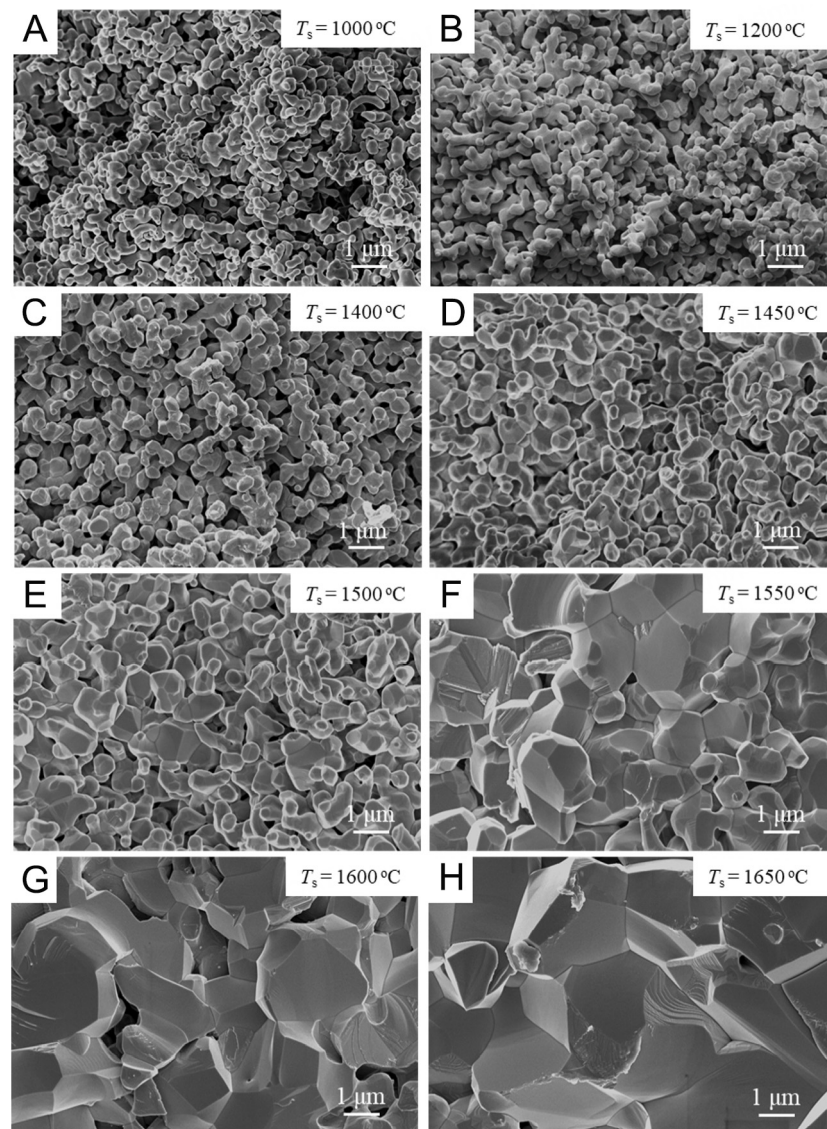


Figure 2. SEM images of fractured surfaces of Al_2O_3 -A ceramics sintered at (A) 1,000 °C, (B) 1,200 °C, (C) 1,400 °C, (D) 1,450 °C, (E) 1,500 °C, (F) 1,550 °C, (G) 1,600 °C, and (H) 1,650 °C.

micrometers are observed in Al_2O_3 -B ceramics, which are formed by decomposing the NH_4HCO_3 large particles as the porogen. As discussed above, the relative density of Al_2O_3 -B ceramics decreases significantly from 78.76% to 48.31% by adjusting the NH_4HCO_3 volume fraction from 20% to 60%. Interestingly, the microstructure far from the large pores in Al_2O_3 -B ceramics depends little on relative density and is similar to that of Al_2O_3 -A ceramic sintered at 1,650 °C. Since the porogen of NH_4HCO_3 is decomposed completely at only 70 °C without any residual or reaction with Al_2O_3 , it is expected to have a limited effect on the sintering characteristics and microstructure of Al_2O_3 -B ceramics except the produced large pores. Therefore, the ceramic connectivity is dominated by the sintering temperature rather than the porogen volume fraction, and the ceramic connectivity is similar for all the Al_2O_3 -B ceramics. Moreover, the ceramic connectivity in Al_2O_3 -B porous ceramic is significantly improved compared to that in Al_2O_3 -A counterpart with a similar density. For example, the ceramic connectivity in Figure 3C is much better than that in Figure 2C, although the corresponding relative density of Al_2O_3 -B (48.31%) is a little lower than that of

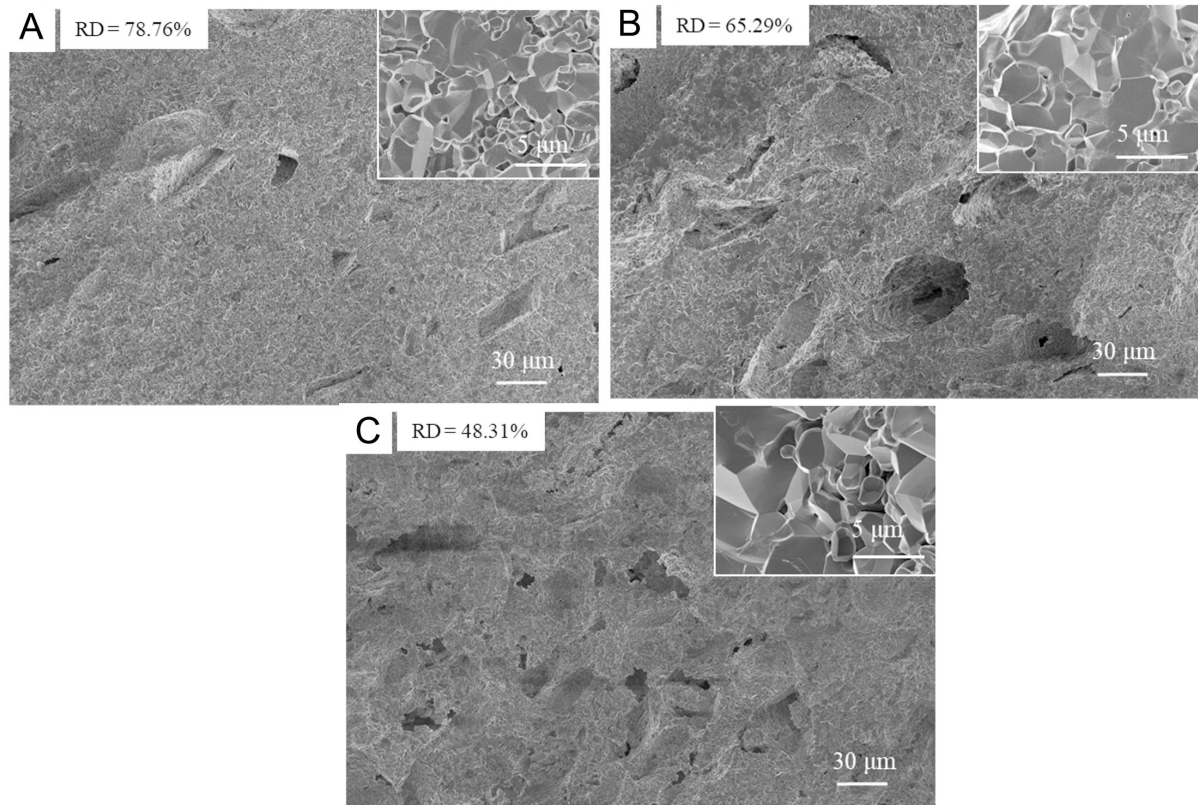


Figure 3. SEM images of fractured surfaces of Al_2O_3 -B ceramics with relative densities of (A) 78.76%, (B) 65.29%, and (C) 48.31%. The insets show the fractured surfaces with higher magnification.

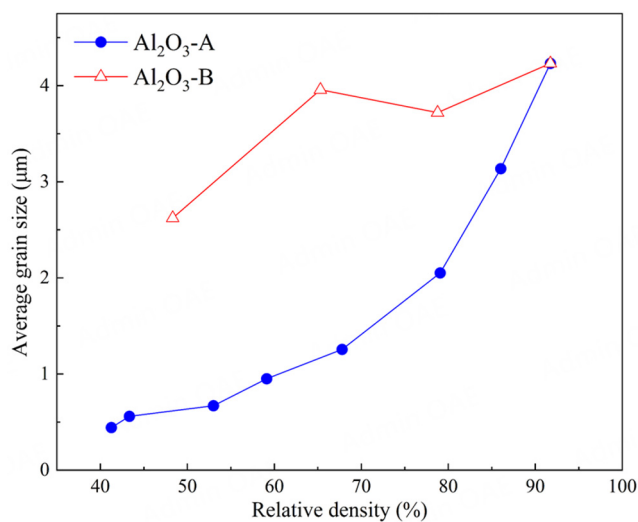


Figure 4. Average grain size of Al_2O_3 -A and Al_2O_3 -B ceramics with different relative densities.

Al_2O_3 -A (53.00%). As shown in Figure 4 and Supplementary Figure 3, the average grain size of Al_2O_3 -B porous ceramics is also higher and more insensitive to relative density compared with Al_2O_3 -A, which is attributed to the higher sintering temperature of 1,650 $^{\circ}\text{C}$ for the former. Figure 5 shows the Vickers hardness as a function of relative density. It is worth noting that the Al_2O_3 -B ceramics are inhomogenous in

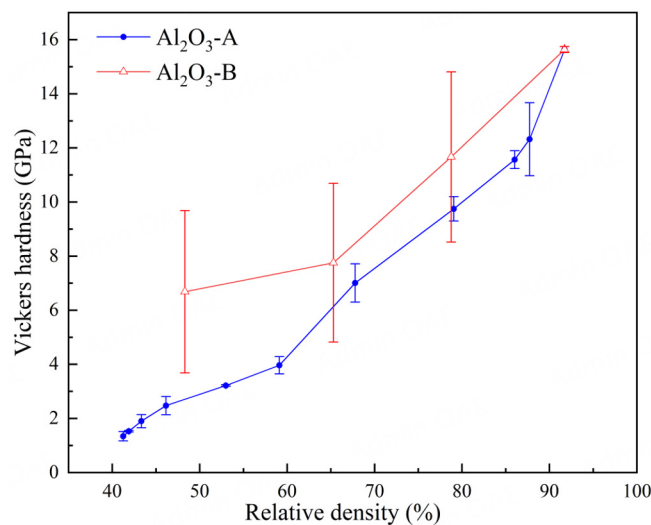


Figure 5. Vickers hardness of Al₂O₃-A and Al₂O₃-B ceramics with different relative densities.

microstructure because of the large pores, so the measurement was conducted in the regions far from the large pores, and the Vickers hardness of Al₂O₃-B ceramics exhibits a much larger deviation compared with Al₂O₃-A. In spite of the large deviation, the Vickers hardness increases with relative density for both the Al₂O₃-A and Al₂O₃-B ceramics, and the latter exhibits a significantly higher Vickers hardness than the former with a similar relative density. The large difference in Vickers hardness is attributed to the different ceramic connectivity between the two groups of ceramics, which is also expected to affect the microwave dielectric properties significantly.

Figure 6A shows the ϵ_r of Al₂O₃-A ceramics sintered at different temperatures. With increasing T_s from 1,000 to 1,300 °C, the ϵ_r increases slightly from 3.00 to 3.49, and it increases more rapidly to 8.99 with further increasing T_s up to 1,650 °C, which is consistent with the relative density shown in Figure 1. The relationship between ϵ_r and relative density for Al₂O₃-A ceramics can be observed more clearly in Figure 6B, where the ϵ_r increases monotonously and smoothly with relative density. Figure 6B also shows that the ϵ_r of Al₂O₃-B ceramics exhibits similar dependence on relative density to Al₂O₃-A counterparts, while the ϵ_r of the former is always slightly higher than that of the latter with a similar relative density, and the difference is larger for the lower relative density. As discussed above, the Al₂O₃-B ceramic exhibits a larger grain size and improved ceramic connectivity than the Al₂O₃-A counterpart with a similar density because of the higher sintering temperature. Since the low-loss microwave dielectric ceramics are generally non-polar materials, their ϵ_r is determined by the electric and ionic polarizations and, hence, insensitive to grain size. Therefore, the larger ϵ_r of Al₂O₃-B ceramics is attributed to better ceramic connectivity. Such results are consistent with those in CaTiO₃ porous ceramic^[32], although the difference in ϵ_r between the two groups of Al₂O₃ ceramics is not so dramatic in the present work. Since CaTiO₃ has a high ϵ_r of 183^[32] and the difference between the ϵ_r of the ceramic phase and air is much larger for the CaTiO₃ porous ceramics, the electric field distribution in the constituting phases is more sensitive to the continuity of ceramic phase, leading to the much stronger dependence of ϵ_r on the ceramic connectivity. Moreover, the ultralow ϵ_r (< 5) can be obtained in both Al₂O₃-A and Al₂O₃-B ceramics when the relative density is lower than 60%, proving the feasibility of achieving ultralow ϵ_r by introducing pores into low- ϵ_r ceramics.

It is well known that the ϵ_r of dielectric composites and porous materials can be predicted by many dielectric mixing rules, including parallel model, serial model, logarithmic model^[45], effective medium approximation

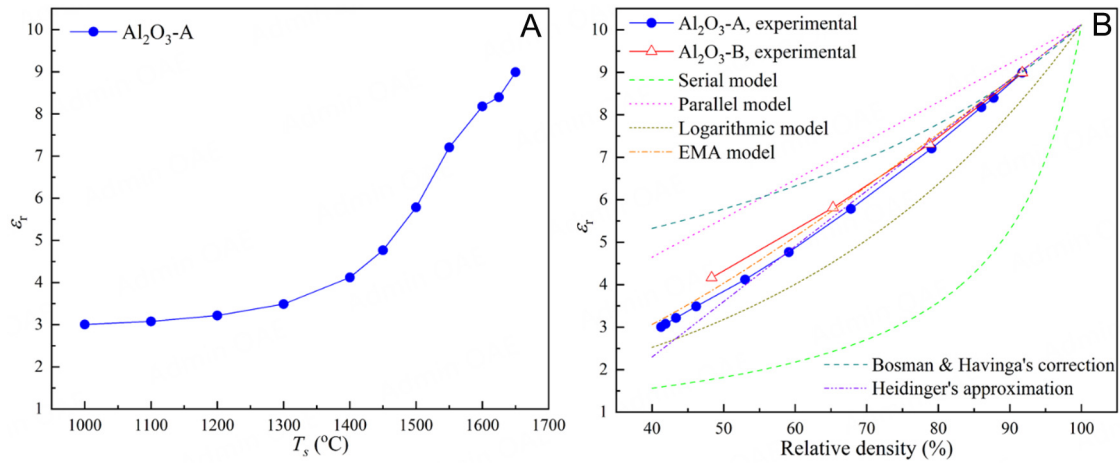


Figure 6. (A) ϵ_r of Al_2O_3 -A ceramics sintered at different T_s . (B) ϵ_r of Al_2O_3 -A and Al_2O_3 -B ceramics with different relative densities and the predicted ϵ_r by several dielectric mixing rules.

(EMA)^[46], Heidinger's approximation^[47], etc. Additionally, Bosman and Havinga's correction^[48] described by

$$\epsilon_{r,\text{theo}} = \epsilon_r (1 + 1.5p) \quad (1)$$

is often used for predicting the dielectric constant of porous materials, where p is the porosity, $\epsilon_{r,\text{theo}}$ is the theoretical dielectric constant of the fully densified material, and ϵ_r is the measured dielectric constant of the material with the porosity p . Bosman and Havinga's correction is usually reliable when the porosity is not high, and the theoretical dielectric constant of Al_2O_3 is calculated to be 10.12 from the measured ϵ_r (8.99) and porosity (8.27%) of Al_2O_3 -A ceramic sintered at 1,650 °C, which is used for the following prediction. Figure 6B shows the predicted ϵ_r of Al_2O_3 porous ceramics with different relative densities from these dielectric mixing rules. The predicted results by the parallel model, serial model, logarithmic model, and Bosman and Havinga's correction differ much from the experimental ones, especially for the low relative density. Although Heidinger's approximation and effective medium approximation provide much better prediction, they still fail to explain the difference between Al_2O_3 -A and Al_2O_3 -B porous ceramics. Such a failure is not surprising, since all the above mixing rules are empirical or based on some assumptions in microstructure, and only the relative density acts as the independent variable. However, the above discussion on microstructure reveals the significant difference in microstructure and ceramic connectivity between Al_2O_3 -A and Al_2O_3 -B ceramics, which should be considered for a more reliable prediction.

Our previous work shows that the parameter α in the exponential model

$$\epsilon_r^\alpha = V_1 \epsilon_{r,1}^\alpha + V_2 \epsilon_{r,2}^\alpha \quad (2)$$

can be used to describe the connectivity of constituting phases in dielectric composites and porous materials^[32], where V is the volume fraction, and the numeric subscripts mean phases 1 and 2. The volume fraction of ceramic phase (phase 1) is just the relative density for porous ceramics, and phase 2 is air with $\epsilon_{r,2} = 1$ and $V_2 = 1 - V_1$, so Eq. (2) can be rewritten as

$$\epsilon_r = V_1 \epsilon_{r,1}^\alpha + (1 - V_1). \quad (3)$$

The fitted parameter α is calculated for the present Al_2O_3 -A and Al_2O_3 -B ceramics from the measured ϵ_r and relative density, and the calculated α as a function of relative density is shown in Figure 7. With increasing T_s from 1,000 to 1,650 °C and relative density from 41.25% to 91.73% for Al_2O_3 -A ceramics, the calculated α increases greatly from 0.162 to 0.488 by about three times. In comparison, Al_2O_3 -B ceramics always exhibit high α values of 0.461–0.478 in spite of the varying relative density from 78.76% to 48.31%, which are very close to the highest α of Al_2O_3 -A ceramic (0.488) sintered at 1,650 °C. Combining with the microstructural analysis shown in Figures 2 and 3, it is clear that the ceramic connectivity and α are dominated by the sintering temperature and insensitive to relative density. As revealed in CaTiO_3 porous ceramics, the improved ceramic connectivity enhances the electric field in ceramic phase and its contribution to the dielectric response of porous ceramics, and therefore increases the final dielectric constant^[32]. Such an effect is similar in Al_2O_3 porous ceramics, although the higher ϵ_r of Al_2O_3 -B than Al_2O_3 -A is not so dramatic compared to the CaTiO_3 porous ceramics due to the much lower ϵ_r of Al_2O_3 (10.12) than CaTiO_3 (183)^[32].

Since Al_2O_3 has a negative τ_f , all the Al_2O_3 -A and Al_2O_3 -B ceramics in the present work exhibit negative τ_f , as shown in Figure 8A and B. With increasing T_s from 1,000 to 1,650 °C and relative density from 41.25% to 91.73% for Al_2O_3 -A, τ_f decreases significantly from -15.8 to -58.5 ppm/°C. In comparison, τ_f decreases more slightly with relative density for Al_2O_3 -B, and the difference between the τ_f values for the relative densities of 48.31% and 91.73% is only 12.7 ppm/°C. Similarly, the parallel model, serial model, and logarithmic model fail in predicting the τ_f of Al_2O_3 porous ceramics. Since ϵ_r is independent of grain size for low-loss microwave dielectric ceramics, as discussed above, its temperature coefficient (τ_ϵ) and, hence, the τ_f are also insensitive to grain size. Therefore, it can be inferred that τ_f is also strongly dependent on ceramic connectivity. The expression for the τ_ϵ of a dielectric composite can be obtained by derivating Equation 2 with respect to temperature as^[32]

$$\tau_\epsilon = \frac{V_1 \epsilon_{r,1}^\alpha \tau_{\epsilon,1} + V_2 \epsilon_{r,2}^\alpha \tau_{\epsilon,2}}{V_1 \epsilon_{r,1}^\alpha + V_2 \epsilon_{r,2}^\alpha} \quad (4)$$

In the present work, phase 2 is air with $V_2 = 1 - V_1$, $\epsilon_{r,2} = 1$, and $\tau_{\epsilon,2} = 0$ for Al_2O_3 porous ceramics. Combining with

$$\tau_f = -\left(\frac{1}{2} \tau_\epsilon + \alpha_L\right) \quad (5)$$

for both the porous and fully dense Al_2O_3 ceramics, the τ_f of the Al_2O_3 porous ceramics can be obtained as

$$\tau_f = \frac{V_1 \epsilon_{r,1}^\alpha \tau_{f,1}}{V_1 \epsilon_{r,1}^\alpha + (1 - V_1)} - \alpha_L. \quad (6)$$

By using $\tau_{f,1} = -60.2$ ppm/°C and $\alpha_{L,1} = 8.1$ ppm/°C for fully dense Al_2O_3 ceramic and assuming that the α_L of porous ceramics is proportional to relative density, the τ_f of Al_2O_3 -A and Al_2O_3 -B porous ceramics can be predicted from the relative density and α , and the results are also shown in Figure 8B. The predicted τ_f decreases with relative density for both Al_2O_3 -A and Al_2O_3 -B ceramics, and Al_2O_3 -A exhibits a higher predicted τ_f than Al_2O_3 -B with similar density, which is consistent with the experimental results and attributed to the poorer ceramic connectivity and lower α for the former. The predicted τ_f values fit the experiments well for all the Al_2O_3 -B porous ceramics and the Al_2O_3 -A counterparts with high relative

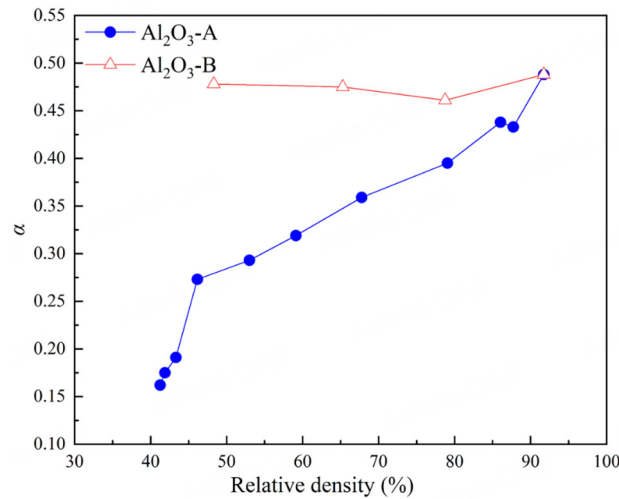


Figure 7. α of Al₂O₃-A and Al₂O₃-B ceramics as a function of relative density.

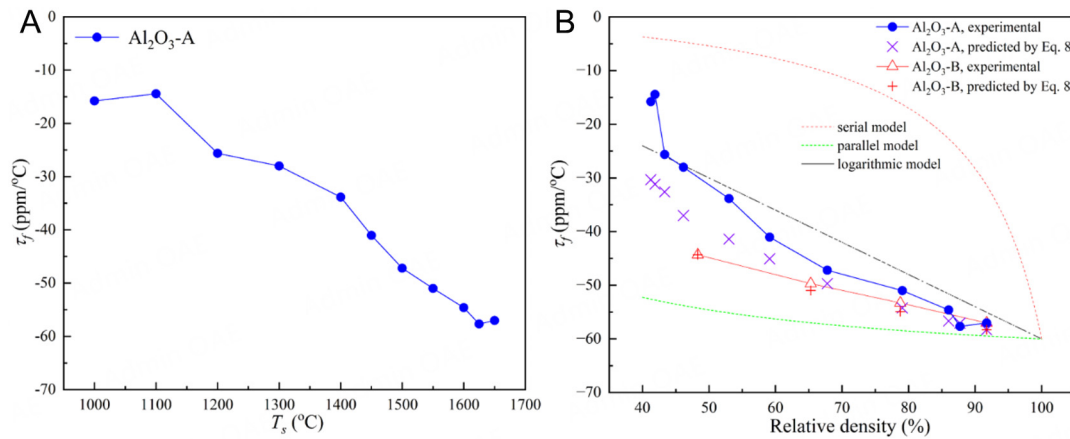


Figure 8. (A) τ_f of Al₂O₃-A ceramics sintered at different T_s . (B) τ_f of Al₂O₃-A and Al₂O₃-B ceramics with different relative densities, and the predicted τ_f by Equation 6 and other dielectric mixing rules.

density. However, when the relative density of Al₂O₃-A ceramics is lower than 60%, the difference between the predicted and experimental results becomes large, indicating that the exponential model is more suitable for predicting the τ_f of Al₂O₃ porous ceramics with relatively good ceramic connectivity. Similarly to ϵ_r , the effect of ceramic connectivity on the τ_f of Al₂O₃ porous ceramics is not so dramatic as that for CaTiO₃^[32] because of the much lower ϵ_r of Al₂O₃ and less sensitive electric field distribution to the continuity of ceramic phase. Additionally, it is well known that the low- ϵ_r microwave dielectric ceramics usually exhibit large negative τ_f values that deteriorate the temperature stability for practical application. The above discussion shows that the pores introduced in microwave dielectric ceramics can not only decrease the dielectric constant, but also improve the temperature stability.

As discussed above, the ϵ_r and τ_f of Al₂O₃ porous ceramics are directly determined by the relative density and ceramic connectivity. In comparison, the Qf value of porous ceramics is more complex since many microstructural factors may result in extrinsic dielectric loss and thus decrease the Qf value. Without considering the effects of microstructural factors, the Qf value of a composite can be expressed as

$$Qf = \left(\frac{V_1 \varepsilon_1^\alpha \frac{1}{Qf_1} + V_2 \varepsilon_2^\alpha \frac{1}{Qf_2}}{V_1 \varepsilon_1^\alpha + V_2 \varepsilon_2^\alpha} \right)^{-1} \quad (7)$$

from the exponential rule^[32]. For the porous ceramics, phase 2 is air with $V_2 = 1 - V_1$, $\varepsilon_{r,2} = 1$, and $\tan \delta_2 = 0$, so the theoretical Qf value of porous ceramics is

$$Qf = \left(1 + \frac{1 - V_1}{V_1} \varepsilon_{r,1}^{-\alpha} \right) Qf_1. \quad (8)$$

By using $\varepsilon_{r,1} = 10.12$ and $Qf_1 = 402,000$ GHz, one can find in [Figure 9A](#) that the predicted Qf value of Al_2O_3 porous ceramics increases as the relative density decreases, since the decreased relative density means the decreased content of lossy Al_2O_3 and increased content of lossless air. However, the measured Qf values of Al_2O_3 porous ceramics are always much lower than that of the dense Al_2O_3 ceramic and the predicted Qf values. Such a contradiction is not surprising since the Qf value of Al_2O_3 itself is very high, and the extrinsic dielectric loss caused by microstructural factors may greatly exceed the ultra-low dielectric loss of Al_2O_3 and hence dominate the dielectric loss and Qf value of Al_2O_3 porous ceramics. Moreover, the Al_2O_3 -B ceramics exhibit similar Qf values of around 40,000 GHz, which are insensitive to the varying relative density from 48.31% to 78.76%, and 1.5-4 times higher than those of the Al_2O_3 -A ceramics with the similar relative densities. Differently from Al_2O_3 -B, the Qf value is strongly dependent on the relative density for Al_2O_3 -A porous ceramics. Such results further verify the dominant role of the microstructural factors. [Supplementary Figure 4](#) also shows the calculated dielectric loss of Al_2O_3 -A porous ceramics at 13 GHz as a function of relative density. Since the Qf value is defined as the product of frequency and reciprocal dielectric loss, the dielectric loss shows a reverse trend to the Qf value. As analyzed from the SEM images, the grain size and ceramic connectivity are the main microstructural factors for the Al_2O_3 -A and Al_2O_3 -B porous ceramics. For Al_2O_3 -A, both the grain size and ceramic connectivity increase with higher sintering temperatures and relative densities. In contrast, for Al_2O_3 -B, these factors remain largely unaffected by changes in relative density. The increase in grain size generally increases the dielectric loss and decreases the Qf value for the dense Al_2O_3 ceramics^[27], which may be responsible for the decreasing Qf value of Al_2O_3 -A ceramics with increasing sintering temperature from 1,000 to 1,300 °C and relative density from 41.25% to 46.15%, as shown in [Figure 9B](#). However, the negative effect of grain size on Qf value is inconsistent with the experimental results for the Al_2O_3 -A ceramics with higher relative densities and Al_2O_3 -B ceramics, which are much more important in the present work. It can be inferred that the Qf value of these ceramics is predominantly determined by the ceramic connectivity, as the ceramic-pore interfaces introduce extrinsic dielectric loss through microwave scattering, and these interfaces can be greatly decreased by enhancing the ceramic connectivity.

By integrating the above discussion on the ε_r , τ_p and Qf value, the optimum microwave dielectric properties with $\varepsilon_r = 4.16$, $Qf = 38,400$ GHz, and $\tau_f = -44.3$ ppm/°C are obtained in Al_2O_3 -B ceramic with a low relative density of 48.31%, indicating that the microwave dielectric properties of ultralow- ε_r porous ceramics can be optimized by regulating both the porosity and ceramic connectivity. Furthermore, the microstructural effects revealed in the present work provide valuable guidance for the future development of ultralow- ε_r porous ceramics. Considering the substantial impact of ceramic connectivity on the Qf value of porous ceramics, good ceramic connectivity is essential for achieving high Qf values. However, the enhanced ceramic connectivity also leads to the increase in both ε_r and $|\tau_f|$, so it is crucial to select the ceramics with both low ε_r and small τ_f in the dense state for obtaining the ultra-low ε_r and improving the temperature stability.

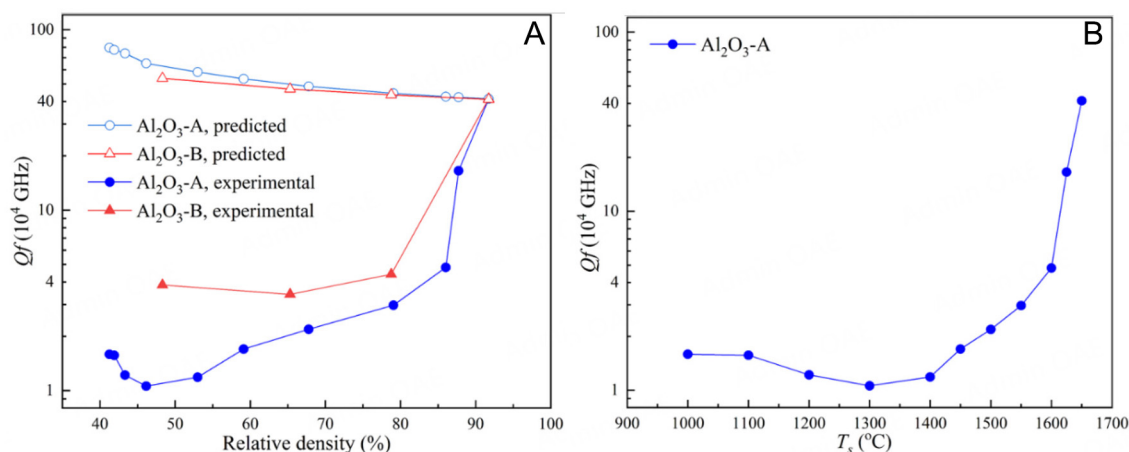


Figure 9. (A) Experimental and predicted Qf values of Al_2O_3 -A and Al_2O_3 -B ceramics with different relative densities. (B) Qf value of Al_2O_3 -A ceramics sintered at different T_s .

CONCLUSIONS

In conclusion, two groups of Al_2O_3 porous ceramics are prepared by incomplete sintering at low temperatures and sintering at the optimal temperature with the introduction of NH_4HCO_3 porogen, respectively. The introduction of pores leads to a significant decrease in ϵ_r , Qf , and $|\tau_f|$, and Al_2O_3 -B ceramic exhibits a slightly higher ϵ_r , a larger $|\tau_f|$, and a much higher Qf value than Al_2O_3 -A with similar density. The microstructural analysis clearly reveals that the ceramic connectivity and relative density of Al_2O_3 -A porous ceramics are improved significantly with increasing sintering temperature, while the excellent ceramic connectivity of Al_2O_3 -B changes little with the porogen content and relative density. The ceramic connectivity is dominated by sintering temperature rather than relative density, and can be described by the parameter α in the exponential rule, which increases significantly with relative density for Al_2O_3 -A but changes little for Al_2O_3 -B. The significantly improved ceramic connectivity in Al_2O_3 -B porous ceramics enhances the contribution of ceramic phase to the ϵ_r and τ_f of porous ceramics, although such effects are not so dramatic as those in $CaTiO_3$ porous ceramics because of the much lower ϵ_r of Al_2O_3 . Moreover, the improved ceramic connectivity increases the Qf value by decreasing the ceramic-pore interfaces that cause extrinsic dielectric loss. The good combination of microwave dielectric properties with $\epsilon_r = 4.16$, $Qf = 38,400$ GHz, and $\tau_f = -44.3$ ppm/°C is obtained in Al_2O_3 -B ceramic with a low relative density of 48.31% and good ceramic connectivity. The important effects of ceramic connectivity revealed in this work contribute to the deep understanding of the tight relationship between microwave dielectric properties and microstructures in porous ceramics, and also inspire the development of ultralow- ϵ_r dielectric materials by regulating both the porosity and ceramic connectivity.

DECLARATIONS

Authors' contributions

Made substantial contributions to the conception and design of the study: Li, L.; Wu, S. Y.

Performed data analysis and interpretation: Yan, X. J.; Cao, M.; Li, L.

Performed data acquisition: Yan, X. J.

Provided administrative, technical, and material support: Li, L.; Chen, X. M.

Availability of data and materials

The data that support the findings of this study are available from the corresponding author upon reasonable request.

Financial support and sponsorship

This work was supported by the National Natural Science Foundation of China under Grant Nos. 52272128 and U20A20243.

Conflicts of interest

All authors declared that there are no conflicts of interest.

Ethical approval and consent to participate

Not applicable.

Consent for publication

Not applicable.

Copyright

© The Author(s) 2025.

REFERENCES

1. Rappaport, T. S.; Sun, S.; Mayzus, R.; et al. Millimeter wave mobile communications for 5G cellular: It will work! *IEEE. Access.* **2013**, *1*, 335-49. [DOI](#)
2. Sebastian, M. T.; Ubic, R.; Jantunen, H. Low-loss dielectric ceramic materials and their properties. *Int. Mater. Rev.* **2015**, *60*, 392-412. [DOI](#)
3. Raveendran, A.; Sebastian, M. T.; Raman, S. Applications of microwave materials: a review. *J. Electron. Mater.* **2019**, *48*, 2601-34. [DOI](#)
4. Li, L.; Zhu, X. L.; Chen, X. M. Where can the low dielectric constant go in dense inorganic materials? *J. Materiomics.* **2023**, *9*, 980-3. [DOI](#)
5. Reaney, I. M.; Iddles, D. Microwave dielectric ceramics for resonators and filters in mobile phone networks. *J. Am. Ceram. Soc. Soc.* **2006**, *89*, 2063-72. [DOI](#)
6. Došler, U.; Kržmanc, M. M.; Suvorov, D. The synthesis and microwave dielectric properties of $\text{Mg}_3\text{B}_2\text{O}_6$ and $\text{Mg}_2\text{B}_2\text{O}_5$ ceramics. *J. Eur. Ceram. Soc.* **2010**, *30*, 413-8. [DOI](#)
7. Chang, S.; Pai, H.; Tseng, C.; Tsai, C. Microwave dielectric properties of ultra-low temperature fired Li_3BO_3 ceramics. *J. Alloy. Compd.* **2017**, *698*, 814-8. [DOI](#)
8. Zhou, D.; Pang, L.; Wang, D.; Qi, Z.; Reaney, I. M. High quality factor, ultralow sintering temperature $\text{Li}_6\text{B}_4\text{O}_9$ microwave dielectric ceramics with ultralow density for antenna substrates. *ACS. Sustain. Chem. Eng.* **2018**, *6*, 11138-43. [DOI](#)
9. Sun, H.; Zhang, Q.; Yang, H.; Zou, J. $(\text{Ca}_{1-x}\text{Mg}_x)\text{SiO}_3$: a low-permittivity microwave dielectric ceramic system. *Mater. Sci. Eng. B.* **2007**, *138*, 46-50. [DOI](#)
10. Bian, J.; Xie, Y. Sintering behavior and dielectric properties of SiO_2 - BPO_4 glass-fluxed ceramics. *J. Eur. Ceram. Soc.* **2018**, *38*, 2747-52. [DOI](#)
11. Kamutzki, F.; Schneider, S.; Barowski, J.; Gurlo, A.; Hanaor, D. A. Silicate dielectric ceramics for millimetre wave applications. *J. Eur. Ceram. Soc.* **2021**, *41*, 3879-94. [DOI](#)
12. Hou, H.; Zhang, A.; Yang, H.; et al. LiGaSiO_4 : an ultra-low permittivity dielectric material enabling application in patch antenna. *Ceram. Int.* **2024**, *50*, 7758-66. [DOI](#)
13. Surendran, K.; Bijumon, P.; Mohanan, P.; Sebastian, M. $(1-x)\text{MgAl}_2\text{O}_4$ - TiO_2 dielectrics for microwave and millimeter wave applications. *Appl. Phys. A.* **2005**, *81*, 823-6. [DOI](#)
14. Wan Jalal, W. N.; Abdullah, H.; Zulfakar, M. S.; Bais, B.; Shaari, S.; Islam, M. T. ZnAl_2O_4 -based microwave dielectric ceramics as GPS patch antenna: a review. *Trans. Indian. Ceram. Soc.* **2013**, *72*, 215-24. [DOI](#)
15. Xie, M.; Li, X.; Lai, Y.; et al. Phase evolution and microwave dielectric properties of high-entropy spinel-type $(\text{Mg}_{0.2}\text{Co}_{0.2}\text{Ni}_{0.2}\text{Li}_{0.4}\text{Zn}_{0.2})\text{Al}_2\text{O}_4$ ceramics. *J. Eur. Ceram. Soc.* **2024**, *44*, 284-92. [DOI](#)
16. Bian, J. J.; Kim, D. W.; Hong, K. S. Microwave dielectric properties of $\text{A}_2\text{P}_2\text{O}_7$ ($\text{A} = \text{Ca}, \text{Sr}, \text{Ba}, \text{Mg}, \text{Zn}, \text{Mn}$). *Jpn. J. Appl. Phys.* **2004**, *43*, 3521. [DOI](#)
17. Thomas, D.; Abhilash, P.; Sebastian, M. T. Casting and characterization of LiMgPO_4 glass free LTCC tape for microwave applications. *J. Eur. Ceram. Soc.* **2013**, *33*, 87-93. [DOI](#)
18. Bian, J.; Sun, X.; Xie, Y. Structural evolution, sintering behavior and microwave dielectric properties of $\text{Al}_{(1-x)}(\text{S}_{10.5}\text{Zn}_{0.5})_x\text{PO}_4$ ceramics. *J. Eur. Ceram. Soc.* **2019**, *39*, 4139-43. [DOI](#)
19. Zhou, D.; Randall, C. A.; Wang, H.; Pang, L.; Yao, X. Microwave dielectric ceramics in Li_2O - Bi_2O_3 - MoO_3 system with ultra-low sintering temperatures. *J. Am. Ceram. Soc.* **2010**, *93*, 1096-100. [DOI](#)

20. Varghese, J.; Siponkoski, T.; Nelo, M.; Sebastian, M. T.; Jantunen, H. Microwave dielectric properties of low-temperature sinterable α -MoO₃. *J. Eur. Ceram. Soc.* **2018**, *38*, 1541-7. [DOI](#)
21. Song, X.; Du, K.; Li, J.; et al. Low-fired fluoride microwave dielectric ceramics with low dielectric loss. *Ceram. Int.* **2019**, *45*, 279-86. [DOI](#)
22. Krupka, J.; Derzakowski, K.; Tobar, M.; Hartnett, J.; Geyer, R. G. Complex permittivity of some ultralow loss dielectric crystals at cryogenic temperatures. *Meas. Sci. Technol.* **1999**, *10*, 387-92. [DOI](#)
23. Li, L.; Fang, Y.; Xiao, Q.; Wu, Y. J.; Wang, N.; Chen, X. M. Microwave dielectric properties of fused silica prepared by different approaches. *Int. J. Appl. Ceram. Technol.* **2014**, *11*, 193-9. [DOI](#)
24. Akkasoglu, U.; Sengul, S.; Arslan, İ.; Ozturk, B.; Cicek, B. Structural, thermal and dielectric properties of low-alkali borosilicate glasses for electronic applications. *J. Mater. Sci. Mater. Electron.* **2021**, *32*, 22629-36. [DOI](#)
25. Wu, S.; Song, K.; Liu, P.; et al. Effect of TiO₂ doping on the structure and microwave dielectric properties of cordierite ceramics. *J. Am. Ceram. Soc.* **2015**, *98*, 1842-7. [DOI](#)
26. Lou, W.; Mao, M.; Song, K.; et al. Low permittivity cordierite-based microwave dielectric ceramics for 5G/6G telecommunications. *J. Eur. Ceram. Soc.* **2022**, *42*, 2820-6. [DOI](#)
27. Penn, S. J.; Alford, N. M.; Templeton, A.; et al. Effect of porosity and grain size on the microwave dielectric properties of sintered alumina. *J. Am. Ceram. Soc.* **1997**, *80*, 1885-8. [DOI](#)
28. Jin, F.; Tong, H.; Shen, L.; Wang, K.; Chu, P. K. Micro-structural and dielectric properties of porous TiO₂ films synthesized on titanium alloys by micro-arc discharge oxidation. *Mater. Chem. Phys.* **2006**, *100*, 31-3. [DOI](#)
29. Xia, Y.; Zeng, Y.; Jiang, D. Dielectric and mechanical properties of porous Si₃N₄ ceramics prepared via low temperature sintering. *Ceram. Int.* **2009**, *35*, 1699-703. [DOI](#)
30. Hou, Z.; Ye, F.; Liu, L. Effects of pore shape and porosity on the dielectric constant of porous β -SiAlON ceramics. *J. Eur. Ceram. Soc.* **2015**, *35*, 4115-20. [DOI](#)
31. Chen, Y.; Guo, W.; Luo, Y.; Ma, Z.; Zhang, L.; Yue, Z. Microwave and terahertz properties of porous Ba₄(Sm,Nd,Bi)_{28/3}Ti₁₈O₅₄ ceramics obtained by sacrificial template method. *J. Am. Ceram. Soc.* **2021**, *104*, 5679-88. [DOI](#)
32. Cao, M.; Li, L.; Wu, S. Y.; Chen, X. M. Dominant role of ceramic connectivity in microwave dielectric properties of porous ceramics. *Acta. Mater.* **2023**, *258*, 119207. [DOI](#)
33. Xu, Y.; Tsai, Y.; Tu, K. N.; et al. Dielectric property and microstructure of a porous polymer material with ultralow dielectric constant. *Appl. Phys. Lett.* **1999**, *75*, 853-5. [DOI](#)
34. Dong, X.; Hu, Y.; Zhao, J.; Wu, Y. Method to predict effective dielectric constant of porous silica low dielectric constant materials. *Phys. B.* **2010**, *405*, 3551-4. [DOI](#)
35. Luo, W.; Guo, J.; Randall, C.; Lanagan, M. Effect of porosity and microstructure on the microwave dielectric properties of rutile. *Mater. Lett.* **2017**, *200*, 101-4. [DOI](#)
36. Meng, F.; Fu, Z.; Zhang, J.; et al. Study on the structure and properties of fine-grained alumina fast sintered with high heating rate. *Mater. Res. Bull.* **2008**, *43*, 3521-8. [DOI](#)
37. Li, L.; Deng, Y.; Chen, G. Status and prospect of garnet/polymer solid composite electrolytes for all-solid-state lithium batteries. *J. Energy. Chem.* **2020**, *50*, 154-77. [DOI](#)
38. Levassort, F.; Lethiecq, M.; Desmare, R.; Hue, T. H. Effective electroelastic moduli of 3-3(0-3) piezocomposites. *IEEE. Trans. Ultrason. Ferroelectr. Freq. Control.* **1999**, *46*, 1028-34. [DOI](#) [PubMed](#)
39. Cao, M.; Yan, X. J.; Li, L.; Wu, S. Y.; Chen, X. M. Obtaining greatly improved dielectric constant in BaTiO₃-epoxy composites with low ceramic volume fraction by enhancing the connectivity of ceramic phase. *ACS. Appl. Mater. Interfaces.* **2022**, *14*, 7039-51. [DOI](#)
40. Alford, N. M.; Penn, S. J. Sintered alumina with low dielectric loss. *J. Appl. Phys.* **1996**, *80*, 5895-8. [DOI](#)
41. Penn, S.; Poole, M.; Breeze, J.; Alford, N. Layered Al₂O₃-TiO₂ composite dielectric resonators with tuneable temperature coefficient for microwave applications. *IEE. Proc. Sci. Meas. Technol.* **2000**, *147*, 269-73. [DOI](#)
42. Kolodiaznyi, T.; Annino, G.; Spreitzer, M.; et al. Development of Al₂O₃-TiO₂Al₂O₃-TiO₂ composite ceramics for high-power millimeter-wave applications. *Acta. Mater.* **2009**, *57*, 3402-9. [DOI](#)
43. Mollá, J.; González, M.; Vila, R.; Ibarra, A. Effect of humidity on microwave dielectric losses of porous alumina. *J. Appl. Phys.* **1999**, *85*, 1727-30. [DOI](#)
44. Kajfez, D.; Gundavajhala, A. Measurement of material properties with a tunable resonant cavity. *Electron. Lett.* **1993**, *29*, 1936-7. [DOI](#)
45. Zakri, T.; Laurent, J.; Vauclin, M. Theoretical evidence for 'Lichtenecker's mixture formulae' based on the effective medium theory. *J. Phys. D. Appl. Phys.* **1998**, *31*, 1589-94. [DOI](#)
46. Stroud, D. Generalized effective-medium approach to the conductivity of an inhomogeneous material. *Phys. Rev. B.* **1975**, *12*, 3368-73. [DOI](#)
47. Heidinger, R.; Nazare, S. Influence of porosity on the dielectric properties of AlN in the range of 30. 40 GHz. *Powder. Metall. Int.* **1988**, *20*, 30-2. Available from: <https://www.osti.gov/etdweb/biblio/6526366> [Last accessed on 6 May 2025]
48. Bosman, A. J.; Havinga, E. E. Temperature dependence of dielectric constants of cubic ionic compounds. *Phys. Rev.* **1963**, *129*, 1593-600. [DOI](#)